Combustion and Flame 255 (2023) 112907

Contents lists available at ScienceDirect

Combustion and Flame

journal homepage: www.elsevier.com/locate/combustflame

Assessing requirements for modeling radiation in diffusion flames using an analytical, non-local model

Guilherme C. Fraga[a,*], Bifen Wu[b], Matthias Ihme[c], Xinyu Zhao[a]

[a] Department of Mechanical Engineering, University of Connecticut, Storrs, CT 06268, United States
[b] Transportation and Power Systems Division, Argonne National Laboratory, Lemont, IL 60439, United States
[c] Department of Mechanical Engineering, Stanford University, Stanford, CA 94305, United States

ARTICLE INFO

Article history:
Received 28 October 2022
Revised 7 June 2023
Accepted 9 June 2023

Keywords:
Radiation modeling
Combustion applications
Non-local model
Non-gray radiative properties
FlameMaster

ABSTRACT

An analytical approach for the calculation of radiative self-absorption in flames is presented, with the objective of providing an effective and computationally inexpensive tool for selecting radiation modeling methods for combustion applications. This one-dimensional non-local model approximates the flame structure as an infinitely long cylinder where all properties vary only along the radial direction. Flamelet solutions are then mapped to the radial direction and the radiative source terms, in particular the absorption, are computed analytically. The model is validated for a laminar jet flame and a turbulent pool fire, with results for the net radiative loss and the flame self-absorption showing good agreement to those of multidimensional, coupled simulations. To illustrate its applicability, the model is employed to study the characteristics of radiation in high-pressure combustion, in fire suppression and in hydrogen combustion. For the pressurized case, increased significance of radiation self-absorption is observed compared to an atmospheric flame, and accounting for the non-gray nature of radiation is found to be critical. In the fire suppression case, comparisons of the S-curves show that the choice of radiation model modifies the lower extinction limit, which becomes more important with reduced oxygen content. Lastly, for the hydrogen flame, the Planck-mean absorption coefficient is found to be more uniformly distributed in the mixture fraction space, and the optical thickness is smaller than a hydrocarbon flame at comparable conditions, indicating that radiation modeling requirements for that flame are likely less stringent. In general, the findings regarding radiation characteristics made on the basis of the non-local model are consistent with observations reported in the literature, but without the need for complex coupled combustion-radiation calculations. Therefore, the model provides a viable approach for selecting appropriate radiation models in combustion simulations.

1. Introduction

Thermal radiation is often the dominant heat transfer mode in many combustion systems, playing an important role in applications such as in fire suppression, high-pressure gas turbine combustors, and sooting flames [1]. Neglecting radiation may lead to significant overestimation of the flame temperature, and inaccuracies in predicting NOx formation, propagation speeds and extinction characteristics (see, e.g., [2–5]). Despite this, numerous analyses of combustion systems still disregard radiative heat transfer, or employ the overly simplistic optically thin or gray medium approaches [6] to reduce the added complexity of including accurate radiation models.

The determination of the radiation field, in particular the radiative absorption, requires the solution of the radiative transfer equation (RTE), which is an integro-differential equation of (usually) six independent variables [7]. Besides, the radiative properties of many common combustion products display an irregular, highly intermittent behavior with respect to the radiation spectrum that must be properly represented [8]. Various methods are available for the solution of the RTE and for the spectral modeling of the radiative properties, spanning a wide range of physical fidelity, accuracy and computational cost [7,9]. In addition, the choice of an adequate RTE solver and spectral model may depend on the geometry of the combustion enclosure and the operating conditions. It is therefore difficult to know *a priori* what combination of solvers and spectral models gives the best compromise between accuracy and cost for a given combustion application, especially for a new geometric configuration or new working conditions.

* Corresponding author.
E-mail addresses: guilherme.fraga@uconn.edu (G.C. Fraga), bifenwu@anl.gov (B. Wu), mihme@stanford.edu (M. Ihme), xinyu.zhao@uconn.edu (X. Zhao).

https://doi.org/10.1016/j.combustflame.2023.112907
0010-2180/

The concept of using a one-dimensional cylinder to represent a diffusion flame for the RTE solution has been recently proposed by Wu et al. [10], based on the physical observation that the high-temperature regions in a flame have a dominant influence on radiation emission, while radiation absorption decays exponentially with increasing optical thickness. Therefore, a model was introduced to approximate the flame as an infinitely long cylinder with only radial variation of species concentrations and temperature, a configuration for which the analytical solution of the RTE can be derived and easily evaluated [11]. This allows taking into account non-local effects in the calculation of the radiative absorption; as such, the model is hereafter referred to as the non-local model for radiation. It has been demonstrated [10] that this one-dimensional model can accurately capture the radiation reabsorption in a small-scale n-heptane turbulent diffusion flame for sooting and non-sooting conditions.

The objective of the present study is to demonstrate the feasibility of using the non-local model to provide radiation modeling recommendations for combustion systems. The model is first presented in Section 2, where it is shown that it can be used alongside any treatment—gray or non-gray—for the radiative properties of the medium. Section 3 is concerned with the validation of the non-local model, which is done by comparing its predictions for the radiative heat source and radiative absorption with those obtained for realistic, multidimensional flames. Arguments for the physical justification of the model are also given in Section 3. Following that, the applicability of the model is illustrated by three examples in Section 4: case 1, consisting of flames under pressurized conditions; case 2, studying extinction limits for reduced oxygen conditions; and case 3, focusing on radiation modeling in hydrogen combustion. Based on the results of these cases, Section 5 provides a general discussion about which conditions the gray medium assumption is, and is not, sufficient for modeling the radiative transfer. Conclusions are finally drawn in Section 6.

2. Radiation modeling in combustion

In simulations of combustion systems, coupling between thermal radiation and the energy equation is achieved through the volumetric radiative heat source S_r, which gives a balance between the local radiative energy absorbed and emitted per unit volume as [7]

$$S_r = \int_0^\infty (\kappa_\eta G_\eta - 4\pi\kappa_\eta I_{b\eta})\mathrm{d}\eta. \tag{1}$$

Here, η is the wavenumber; κ_η is the spectral absorption coefficient, a property of the medium that is typically dependent on the wavenumber, temperature, pressure, and medium composition; $I_{b\eta}$ is the spectral blackbody radiative intensity, determined from Planck's law; and G_η is the incident spectral radiation, defined as the integration of the local spectral radiative intensity I_η over all solid angles Ω, $G_\eta = \int_{4\pi} I_\eta \mathrm{d}\Omega$.

The determination of the spectral intensity requires the solution of the radiative transfer equation (RTE). For typical combustion products without radiation scattering, the RTE reduces to

$$\frac{\mathrm{d}I_\eta}{\mathrm{d}s} = -\kappa_\eta I_\eta + \kappa_\eta I_{b\eta}, \tag{2}$$

where s is the coordinate along the path of radiation propagation. In principle, this equation involves five dimensions (three spatial and two directional coordinates), thus solving it can be computationally expensive. In the present study, this is carried out by considering an idealized cylindrical configuration, for which an analytical solution of the RTE is available [11], as described in Section 2.1.

An additional challenge in modeling radiative transfer concerns the integration over the wavenumber spectrum in Eq. (1). As long as sufficiently detailed information of κ_η is available, this integral can be evaluated with a high degree of accuracy. However, for common gaseous combustion products, κ_η displays a highly irregular dependence on η, characterized by millions of absorption lines, which makes the line-by-line (LBL) solution of the radiation field extremely costly and prohibitive for most practical applications. This gives rise to models that ultimately aim to perform the spectral integration in a more computationally efficient manner.

If the participating medium is assumed to be gray, spectral variations of the absorption coefficient are neglected, so $\kappa_\eta = \kappa$ for any η. Hence, Eqs. (1) and (2) can be simplified to

$$S_r = \kappa G - 4\pi\kappa I_b, \tag{3}$$

$$\frac{\mathrm{d}I}{\mathrm{d}s} = -\kappa I + \kappa I_b, \tag{4}$$

where $I_b = \int_0^\infty I_{b\eta}\mathrm{d}\eta$, $G = \int_{4\pi} I\mathrm{d}\Omega$, and the gray absorption coefficient κ is usually taken as the Planck-mean absorption coefficient $\kappa_P = \int_0^\infty \kappa_\eta I_{b\eta}\mathrm{d}\eta/I_b$. An advantage of the gray medium approach is that the RTE needs to be solved only once for each optical path, which greatly reduces the computational cost of determining the radiation field. However, it is well-recognized that a gray medium approximation often yields large errors in the prediction of radiative heat sources and heat fluxes, especially when gas radiation is dominant [12–15].

To capture the spectral dependence of the radiative properties, several non-gray spectral models are available in the literature [7–9]. In the present study, the weighted-sum-of-gray-gases (WSGG) model is chosen for this purpose. The WSGG model represents the non-gray medium as a small set of gray gases that occupy a fixed, non-contiguous portion of the spectrum. Each gas j is assigned an absorption coefficient κ_j, independent of the wavenumber, and a weighting coefficient w_j, corresponding to the fraction of blackbody energy lying within the spectral regions $\Delta\eta_j$ occupied by the gas. Integrating Eq. (2) over $\Delta\eta_j$ yields [16]

$$\frac{\mathrm{d}I_j}{\mathrm{d}s} = -\kappa_j I_j + \kappa_j w_j I_b, \tag{5}$$

which can be solved individually for each gas j to determine the partial radiative intensity I_j. Once this is conducted for all J gray gases in the model, the radiative heat source is computed as

$$S_r = \sum_{j=1}^{J} (\kappa_j G_j - 4\pi\kappa_j w_j I_b). \tag{6}$$

with $G_j = \int_{4\pi} I_j \mathrm{d}\Omega$.

The dependence of the WSGG coefficients w_j and κ_j on the thermodynamic state for each gas j is obtained here from the correlations of Bordbar et al. [17] for the atmospheric heptane and methane flames, and of Bordbar et al. [18] for the high-pressure flames. These correlations are applicable to H_2O-CO_2 mixtures with mole fraction ratios varying between 0.01 and 4.0, which encompasses the conditions examined in the present study. Because the correlations of [17,18] are applicable to a pure-H_2O participating medium, the H_2O WSGG correlations of Coelho and França [19] are used for the hydrogen flame instead.

2.1. The one-dimensional, non-local model

In the non-local model, the radiative heat transfer is assumed to take place in a one-dimensional cylindrical configuration that is constructed from appropriate laminar flamelet profiles, as illustrated in Fig. 1(a). The fuel and air streams are respectively located inside and outside the stoichiometric radial position $r = r_{st}$ (configurations that represent other types of diffusion flames and premixed flames can be set up using corresponding flamelets). There are no variations of the properties along the azimuthal and axial

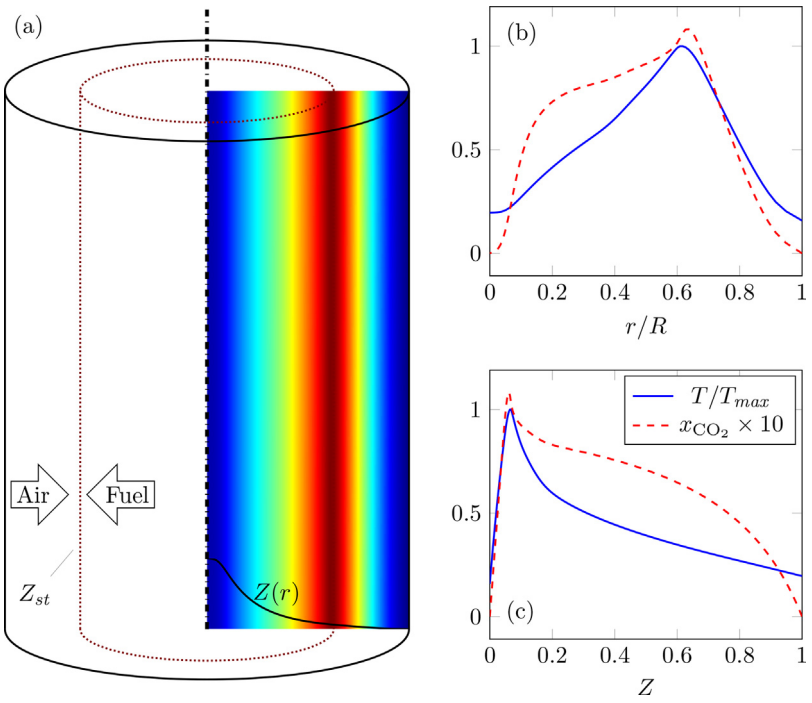

Fig. 1. (a): Schematic of the geometrical configuration constructed in the non-local model, superimposed by the iso-contours of temperature along a cross-section. (b) and (c): Profiles of temperature and CO_2 mole fraction in the physical and mixture fraction spaces.

directions. Mapping between the composition (Z) and physical (r) spaces is given by

$$r(Z) = \int_{Z'\big|_{r=0}=1}^{Z'=Z} \sqrt{\frac{2D}{\chi}}\,\mathrm{d}Z', \tag{7}$$

where D and χ are the thermal diffusivity and the scalar dissipation rate evaluated at position Z' in the mixture fraction space, respectively. By construction, the mixture fraction at the cylinder border, $r = R$, is equal to zero. An example of the mapping of the temperature and CO_2 mole fraction between mixture fraction and physical spaces is provided in Fig. 1(b) and (c). A discussion on the effects of varying the radius of the cylinder is provided in Appendix A.

The RTE, with scattering neglected, may be expressed in a general form as

$$\frac{\mathrm{d}I}{\mathrm{d}s} = -aI + aS_b, \tag{8}$$

where for a gray medium, for a non-gray medium in the framework of the WSGG model, and for the RTE in spectral form the coefficients a and S_b can be written as

$$\text{Gray medium:} \quad I \to I, \quad a \to \kappa, \quad S_b \to I_b \tag{9}$$

$$\text{WSGG model:} \quad I \to I_j, \quad a \to \kappa_j, \quad S_b \to w_j I_b, \tag{10}$$

$$\text{Spectral form:} \quad I \to I_\eta, \quad a \to \kappa_\eta, \quad S_b \to I_{b\eta}. \tag{11}$$

Equation (8) integrated along s yields

$$I = I_w \exp(-\tau_s) + \int_0^{\tau_s} S_b \exp[-(\tau_s - \tau_s')]\mathrm{d}\tau_s'. \tag{12}$$

where I_w is the radiative intensity at the cylinder border, which is taken to be zero in the present analyses (since at the outer cylinder surface the air stream is cold and lacks participating species). In Eq. (12), the s-space has been transformed into τ_s-space, the determination of which is the central challenge of the one-dimensional non-local model, as shown below. The derivation presented next, which is carried out in terms of Eq. (12), holds true for either gray or non-gray media by selecting appropriate a and S_b.

The radiative intensity (and ultimately, the incident radiation) is solved from Eq. (12) for a cylindrical configuration with radius R, as illustrated in Fig. 2. The temperature and radiative properties vary only in the radial direction, $T = T(r)$, $a = a(r)$ and $S_b = S_b(r)$. At any point P, the radiative intensity traveling along direction s is denoted $I(r_P, \theta, \psi)$, where r_P is the distance of P to the cylinder axis, θ is the angle that the vector s forms with the axis, and ψ is the angle (measured in a plane normal to the cylinder axis) between s and the vector that connects P to the axis. In this framework, τ_s in Eq. (12) is the optical thickness measured along s from the cylinder border P_0 to P. Hence, denoting τ and τ_0 as the optical thicknesses measured from the cylinder axis to P and to P_0 respectively (both in the $r-\psi$ plane, see Fig. 2), from trigonometric relations it can be established that $\tau_s = (\tau\cos\psi + \sqrt{\tau_0^2 - \tau^2\sin^2\psi})/\sin\theta$, where $\tau = \int_0^{r_P} a(r)\mathrm{d}r$ and $\tau_0 = \int_0^R a(r)\mathrm{d}r$.

Consider now a point P' located somewhere along s, characterized by an angle ψ' and a radial position $r_{P'}$. An optical thickness τ' can be defined in a similar manner to τ, $\tau' = \int_0^{r_{P'}} a(r)\mathrm{d}r$, from which expressions for τ_s' (which is analogous to τ_s, but for point P'), $\tau_s - \tau_s'$ and $\mathrm{d}\tau_s'$ can be obtained. Substituting these into Eq. (12) yields the following equations for I in terms of τ, τ' and τ_0 only: for $-\pi/2 \le \psi < \pi/2$,

$$\begin{aligned} I = &\int_{\tau|\sin\psi|}^{\tau_0} S_b \frac{\tau'/\tau}{\sin\theta\sqrt{(\tau'/\tau)^2 - \sin^2\psi}} \\ &\times \exp[\frac{1}{\sin\theta}(\tau\cos\psi + \sqrt{\tau'^2 - \tau^2\sin^2\psi})]\mathrm{d}\tau' \\ &+ \int_{\tau|\sin\psi|}^{\tau} S_b \frac{\tau'/\tau}{\sin\theta\sqrt{(\tau'/\tau)^2 - \sin^2\psi}} \\ &\times \exp[\frac{1}{\sin\theta}(\tau\cos\psi - \sqrt{\tau'^2 - \tau^2\sin^2\psi})]\mathrm{d}\tau'; \end{aligned} \tag{13}$$

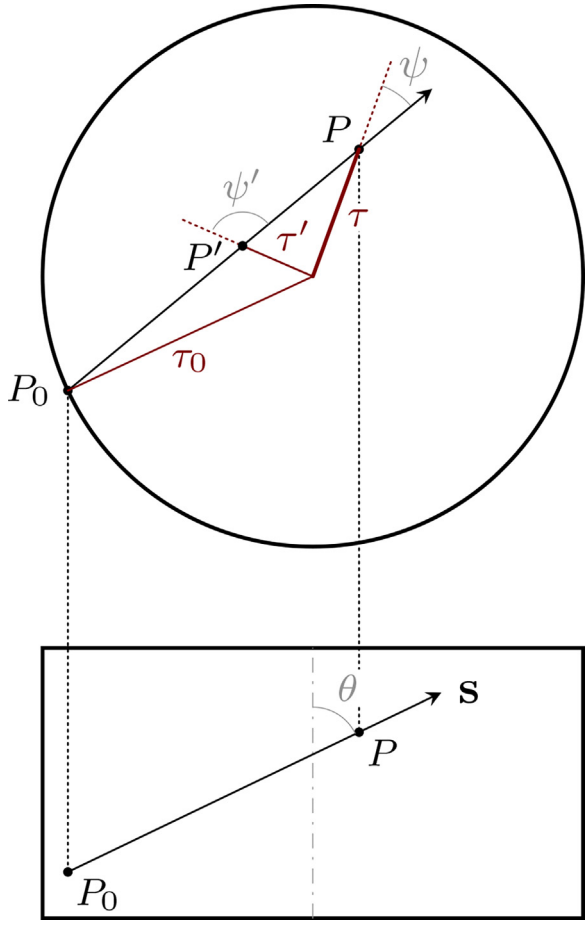

Fig. 2. Coordinate systems used in the derivation of the non-local model (top and side views).

and, for $\pi/2 \leq \psi < 3\pi/2$,

$$I = \int_{\tau}^{\tau_0} S_b \frac{\tau'/\tau}{\sin\theta\sqrt{(\tau'/\tau)^2 - \sin^2\psi}} \times \exp[\frac{1}{\sin\theta}(\tau\cos\psi + \sqrt{\tau'^2 - \tau^2\sin^2\psi})]\mathrm{d}\tau'. \quad (14)$$

The incident radiation is then determined by integrating the resulting I along the ψ and θ directions,

$$G = \int_0^{\pi}\int_0^{2\pi} I\sin\theta\,\mathrm{d}\psi\,\mathrm{d}\theta. \quad (15)$$

This integration is carried out numerically using an in-house procedure. The numerical code employed in the present study to determine the incident radiation is made available at https://github.uconn.edu/CTF-UConn/CylinderModel.git. The numerical code can be used as a standalone program without coupling to any combustion solver, provided that one-dimensional, flamelet-like solutions are given as input.

2.2. Coupling of the model to a combustion solver

While the non-local model may be used to determine the radiative absorption through decoupled calculations, as it is done in the validation study reported in Section 3.1, the main utility of the model lies in approximating self-absorption in coupled Computational Fluid Dynamics (CFD) simulations of combustion systems. In standard coupled thermal radiation-combustion simulations, the RTE is solved from predetermined composition fields—i.e., temperature and mole fractions of the participating species—at the start of any new iteration or time step. The resulting S_r field is then fed back as a source term into the energy equation, which is solved (along all other relevant transport equations) in order to update the aforementioned scalars, and the process is repeated until a convergence criterion is met.

The non-local model has the advantage of not requiring the knowledge of the composition fields in the CFD domain for the solution of the radiation field. Rather, at any given location of the CFD domain, the model only needs to be provided with the local flamelet profile, from which the mapping to the r-space is carried out following Eq. (7), and the local G is computed from Eqs. (13) to (15). From this, the local (to that particular CFD cell) self-absorption and radiative loss are determined. The procedure is repeated for each CFD cell to yield the full S_r, which, for a coupled calculation, is returned into the energy equation as described previously.

3. Validation and physical justification of the non-local model

3.1. Validation

To demonstrate the accuracy of the one-dimensional non-local model, radiation fields predicted by the model are compared in this section to those determined by realistic (in terms of geometry), multidimensional numerical simulations. A modified "Santoro" methane/air co-flow diffusion flame is considered; details on the geometry and operating conditions are provided in Miguel et al. [20]. The baseline simulations for the present analyses were carried out [21] in a coupled combustion-radiation laminar flame solver, using a 16-species skeletal chemical mechanism [22] and a mixture-averaged transport property model. Thermal radiation was solved by a forward Photon Monte Carlo method coupled to either a gray model (with the Planck-mean absorption coefficient pretabulated from the HITEMP2010 database [23]) or a LBL spectral radiative property model [24]. More information on the simulation setup and validation of the numerical results are given in Ref. [21].

Essential thermochemical scalar fields, including temperature and concentrations of radiatively participating species, are taken from the results of the multidimensional simulations using a Lagrangian flamelet extraction method [10,25] and serve as input to the non-local model. Radiation is then solved in a decoupled manner to combustion. The upper row of plots in Fig. 3 compares the net radiative loss (emission minus absorption, or $-S_r$) computed by the non-local model to that obtained directly from the multidimensional simulation. Radial profiles are shown at three heights x above the burner within the flame region (the flame height was measured experimentally to be 76 mm).

The agreement between the model and the simulation is excellent for the three heights and for both gray and non-gray solutions (the same gray and non-gray approaches used in the multidimensional simulations were employed for the calculations with the non-local model). Comparisons between the model and the reference in terms of the radiative absorption have also been performed, and are reported in the bottom rows of Fig. 3. Because emission is dependent only on local quantities and can be easily approximated, values of absorption are more significantly influenced by the simplifying assumptions of the non-local model than those of net loss. Nevertheless, Fig. 3 shows that the model retains a good level of accuracy for computing the local absorption across all heights and most radial positions.

Further validation of the non-local model was presented in Ref. [10] for a 7.1 cm-diameter heptane pool fire. The measured height of the flame was 34.5 cm, showing a transition between the laminar and turbulent regimes. The puffing frequency was determined [10] to be 5.87 Hz, and instantaneous contours of the flame temperature evidence an asymmetric flame shape. The analysis in

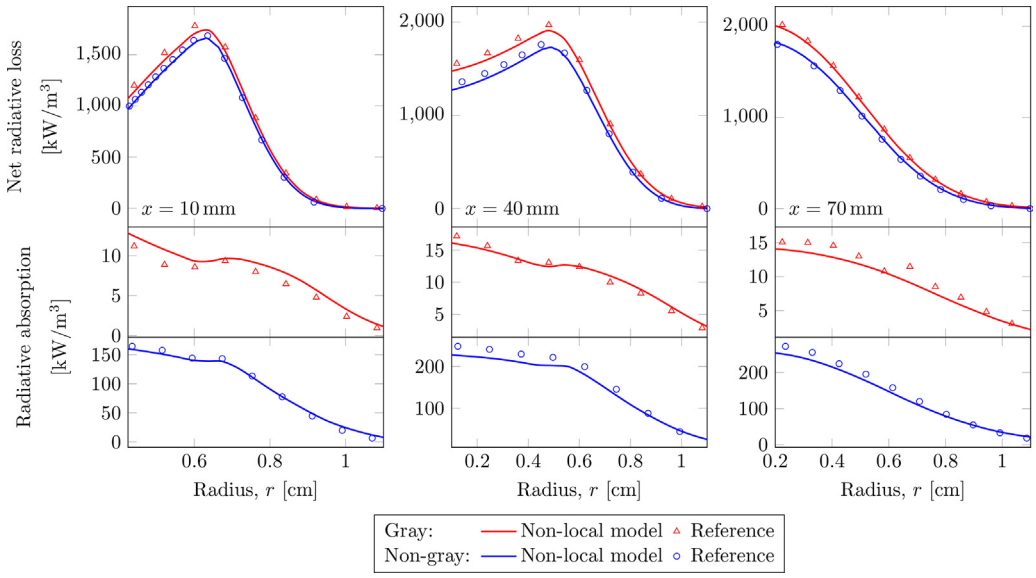

Fig. 3. Comparison of the net radiative loss and radiative absorption obtained from the non-local model and results extracted from an axisymmetric simulation of a stable laminar diffusion flame [21].

Wu et al. [10] was similar to the one reported here, with profiles of radiative self-absorption extracted from highly-resolved, multi-dimensional simulations and compared to results of the non-local model. Conditions of radiation with and without considering soot were considered at different flame heights. In general, good agreement between the non-local model and the multidimensional simulations was observed.

3.2. Physical justification for the non-local model

The good performance of the non-local model for the laminar and pool-fire configurations, despite of its very simple representation of flame as a one-dimensional cylinder, may be explained by the characteristics of the radiative emission and absorption in typical diffusion flames. Firstly, emission depends on the temperature raised to the fourth power through the blackbody intensity I_b. Therefore, strong emission in a flame is confined to a narrow region in the vicinity of the flame surface. For example, for the laminar flame considered in Section 3.1, the temperature drops from 2000 K to 1400 K within a short distance of 5 mm. Correspondingly, I_b (and, to a first approximation, the radiative emission as well) reduces by a factor of four. Therefore, the majority of the emission is captured by including in the model the appropriate temperature and species concentrations profiles in the flame region.

On the other hand, the radiative intensity decays exponentially with the optical thickness according to Beer's law [6] and G is directly related to the intensity. As long as the optical thickness in the inner region of the flame is negligible, the optical thickness is well represented by including the flame ring, as is done in the model. The size of the inner radius of this ring is not important for determining the optical thickness and the incident radiation, as long as the size of the ring itself is maintained, as demonstrated in Appendix A. Thus, it is more convenient to replace the flame ring geometry by a cylinder, for which an analytical solution of the RTE is available.

From this reasoning, we see that, as long as the major emission and absorption contributors are included, the actual geometric shape of the flame is less relevant for capturing the radiative absorption near the high-temperature regions. However, this is conditioned on the assumptions that there is a large temperature inhomogeneity in a narrow flame front, and that the center of the flame (i.e., the region confined inside the flame ring) does not contribute significantly to the optical thickness. The former may not be the case in applications such as MILD combustion, for example; and the latter, for large flames, where the greater length scales increase the optical thickness at the center of the flame. Testing of the non-local model for those scenarios is still required, and care must taken when applying the model to them.

4. Example applications

The non-local model is used in this section to study three example combustion configurations involving one-dimensional, laminar, counterflow diffusion flames at different combustion conditions. All calculations are carried out in the flame simulation toolbox FlameMaster [26], into which gray and non-gray instances of the non-local model are implemented. The τ, θ and ϕ integrations needed to solve Eqs. 13–(15) are performed numerically though a trapezoidal scheme considering forty-one equally-spaced quadrature points along each dimension; further refining the discretization did not significantly impact the results. Coupling of radiation to the energy equation follows the procedure described in Section 2.2.

For any given value of stoichiometric scalar dissipation rate χ_{st}, FlameMaster solves the one-dimensional, laminar flame structure in the Z-space. By varying χ_{st}, S-curves of the maximum flame temperature $T_{\max}$ as a function of the scalar dissipation rate are produced. In all cases, the temperatures of the fuel and air streams are assumed to be 371 K and 300 K, respectively. Two fuels are studied, heptane and hydrogen, to represent both traditional hydrocarbon-fueled and sustainable hydrogen-fueled applications. Combustion of the former is represented by a 33-species skeletal mechanism [27]; a 9-species mechanism [28] is employed for the latter. Soot formation and soot radiation are not considered in any of the calculations.

4.1. Case 1: high-pressure flames

Combustion within gas turbine combustors and internal combustion engines often take place under pressurized conditions. Higher pressures tend to enhance the importance of the radiative exchange by increasing the optical thickness of the medium

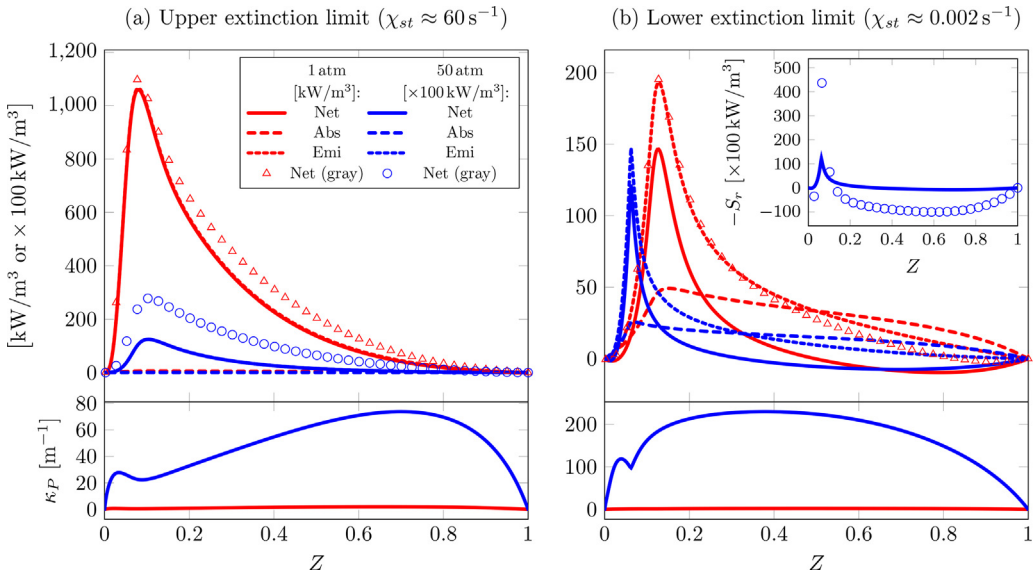

Fig. 4. Radiative emission, absorption and net loss for an atmospheric and pressurized heptane flame near (a) the upper and (b) lower extinction limits. Results correspond to the non-gray medium, unless explicitly stated.

Table 1
Optical thickness and flame width estimates for the atmospheric and high-pressure conditions in Fig. 4.

	Upper extinction		Lower extinction	
	1 atm	50 atm	1 atm	50 atm
τ [–]	0.001	0.004	0.15	2.4
R [cm]	0.1	0.01	11.3	1.9

[6]. To understand the radiation characteristics under pressurized conditions, two heptane flames are considered, one at atmospheric pressure and the other at 50 atm. These flames were simulated from the lower (i.e., heat loss-controlled) to the upper (strain rate-controlled) extinction limits considering gray and non-gray radiation. In this section, only the radiation field near extinction is discussed.

Figure 4 shows the emission, absorption and net radiative loss as a function of the mixture fraction for the two flames at conditions near the upper (corresponding to a stoichiometric scalar dissipation rate $\chi_{st} \approx 60$ s^{-1}) and lower ($\chi_{st} \approx 0.002$ s^{-1}) extinction limits using the non-gray WSGG model. The net radiative loss from the gray solution is also shown for comparison purposes. The pressurized flame displays far greater radiation emission and net loss than the atmospheric flame (note that the units of the data in Fig. 4 for the two pressures are different). As for absorption, while it is negligible for both atmospheric and pressurized flames near the upper extinction limit—leading to virtually equal emission and net loss—that is not the case near the lower extinction limit. This is explained by observing the optical thickness of each flame, which for the purposes of this analysis may be defined as $\tau = \int_0^R \kappa_P \mathrm{d}r$, where the local Planck-mean absorption coefficient is also plotted in Fig. 4. Values of τ for the two pressure and two conditions in Fig. 4 are reported in Table 1, showing that there is an appreciable increase in the optical thickness (by up to three orders of magnitude) from the upper to the lower extinction limits, which leads to an increase in the radiative self-absorption by the flame.

The optical thickness is directly proportional to the Planck-mean absorption coefficient, which is much larger for the 50 atm flame (due to the approximately linear relation between κ_P and the partial pressure of the participating species) and near the lower extinction limit (due to the relatively lower temperatures at this limit, cf. the S-curves in Figs. 5 and 6). The value of τ is also influenced by the total radius R of the physical domain, which is related to the flame thickness. Values of R for each condition considered in this section are also reported in Table 1. Near the upper extinction limit, the larger strain rate severely reduces the flame thickness and R is small. Conversely, as one approaches the lower extinction limit, the flame gets broader and R increases significantly for both low and high-pressure cases. Increasing the pressure reduces the flame thickness and hence R, as expected, but this effect is counteracted by the increase in κ_P, resulting in a net increase in the optical thickness for pressurized conditions compared to the 1 atm flames. The differences in the flame thicknesses also explain why self-absorption is far more important for the 1 atm flame at the lower extinction limit than for the 50 atm flame at the upper extinction limit, even though the Planck-mean absorption coefficient of the latter is much larger than that of the former. The present findings regarding the impact that increasing pressure has on the optical thickness and the radiative transfer of the flame are consistent with what is reported in the literature (for instance, see [29,30]).

Figure 4 also compares the net radiative loss predicted by assuming gray (the solid lines with markers) and non-gray media. The emission and absorption for the gray calculation are omitted for clarity. Minor differences between the gray and non-gray models are observed at 1 atm near the upper extinction limit, with approximately 3.5% difference near the region of maximum radiative loss. However, the accuracy of the gray assumption is significantly poorer for the other configurations considered in Fig. 4. In general, the gray model has a worse performance for the pressurized flame than for the atmospheric flame. In the case of the former, the gray assumption overestimates the maximum net radiative loss by a factor of 2.2 at the upper extinction limit; at the lower extinction limit, this factor increases to almost 4.0. These observations are consistent with radiation studies in internal combustion engines [31] and gas turbine engines [32]. Nonetheless, it is worth noting that any inaccuracy of the gray model is less important for the overall calculation of the flame temperature and structure as one approaches the upper extinction limit, due to the smaller contribution from radiation to the energy equation. This is further discussed in Section 5.

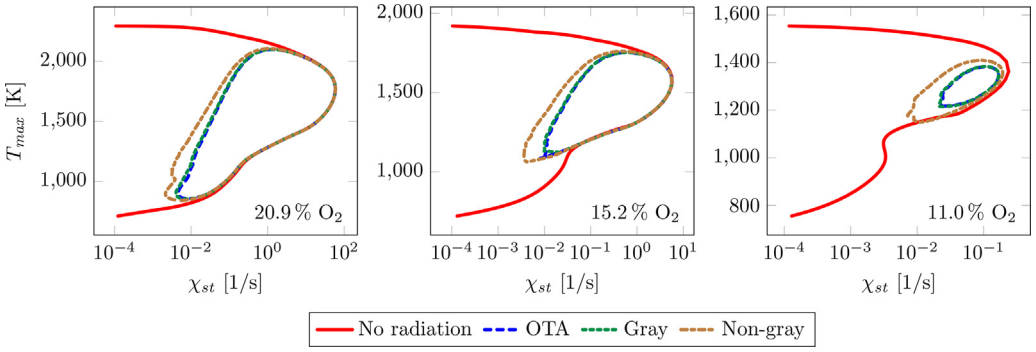

Fig. 5. S-curves for the reduced oxygen (atmospheric) flames.

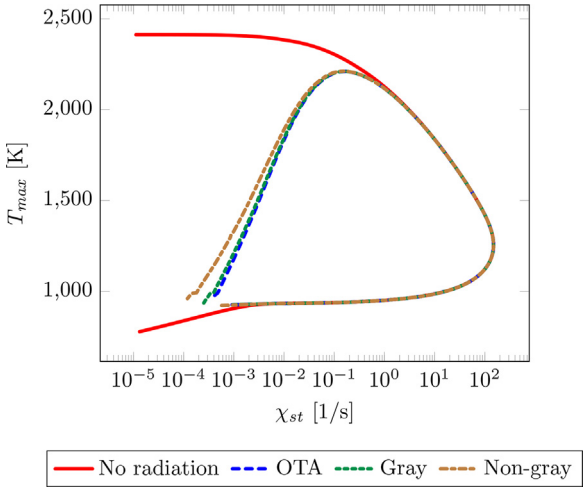

Fig. 6. S-curves for the hydrogen flame.

4.2. Case 2: extinction limit under reduced oxygen conditions

In addition to the radiative loss, the extinction behavior of flames is also influenced by reduced oxygen levels, which is a scenario of great relevance for fire safety [33]. In order to investigate the interplay between radiation and oxygen dilution, this section examines atmospheric heptane flames burning with three different oxygen concentrations in the oxidizer stream: 20.9% in volume concentration (standard air), 15.2% and 11.0%. In particular, the impact of radiation modeling on the extinction limits is studied here.

Figure 5 shows S-curves for the three flames. Each point along the curve represents a one-dimensional counterflow flame solution, where $T_{\max}$ is the maximum temperature in the domain and χ_{st} is the corresponding stoichiometric scalar dissipation rate for that particular solution. Besides results obtained with the gray and non-gray non-local model, the figure also includes S-curves produced by neglecting radiative loss and by computing it using the optically thin approximation (OTA). The latter is a common treatment for radiation in combustion simulations, and consists of foregoing the solution of the RTE by considering only the radiative emission term [1]. All flames are subjected to atmospheric pressure.

Above a sufficiently large value of χ_{st}, the different radiation modeling approaches lead to very similar S-curves, and all models yield almost identical upper extinction points except for the 11.0% O_2 case. This indicates that the contribution from thermal radiation to the flame structure is mostly negligible at high scalar dissipation rates (see also Section 5). However, this contribution becomes increasingly important when oxygen concentrations are reduced, and therefore an accurate radiation treatment becomes correspondingly more important. For the 11.0% O_2 flame, there is a visible difference in the upper extinction limit predicted by the no radiation, gray and non-gray calculations.

As χ_{st} decreases, the error of neglecting radiation becomes increasingly larger for all oxygen concentrations. The OTA and the gray model predict similar shapes for the S-curve, even at small stoichiometric scalar dissipation rates, which is further evidence of the limitations of the gray model in accurately capturing the radiation field near the lower extinction limit. As shown in Fig. 4, the gray solution near the lower extinction limit at 1 atm overestimates the total radiative loss and underestimates absorption, which brings its results closer to those of the OTA calculation, where no self-absorption is accounted for.

4.3. Case 3: hydrogen flames

The final combustion scenario compares the previously discussed atmospheric heptane/standard air flame in Sections 4.1 and 4.2 to an atmospheric hydrogen/air counterflow diffusion flame. A unique feature of hydrogen combustion is that CO_2, which is often the strongest contributor to radiation emission and absorption in engine combustion [31], is not present. Therefore, with the recent interest in hydrogen-powered gas turbine engine combustion, it is important to understand how radiation characteristics change in such combustion systems, and whether existing radiation modeling approaches are still valid in hydrogen-powered combustors.

The S-curve for the hydrogen flame as computed by different radiation treatments is reported in Fig. 6, and shows the same trends as the S-curves of the heptane flames in Fig. 5. However, the departure between the gray and non-gray solutions near the lower extinction limit is smaller for the hydrogen flame than it is for the flames in Fig. 5. For comparison, the difference in the stoichiometric scalar dissipation rate at the lower extinction point for the hydrogen flame is no more than 0.0002 s^{-1}, less than a third of the corresponding difference for the 20.9% O_2 heptane flame.

Figure 7 plots the profiles of the radiative emission, absorption and the net radiative loss for the heptane and hydrogen flames for $\chi_{st} = 1$ s^{-1} at the upper branch of the S-curve, which corresponds approximately to the largest $T_{\max}$ value (and, therefore, largest radiative loss) of both flames. The radiative loss is larger for the heptane flame than for the hydrogen one; this trend is observed throughout the upper branch of the S-curve, as evidenced by the fact that the $T_{\max}$ is greater for the former flame (compare the leftmost plot of Figs. 5 and 6). Self-absorption is also larger for the heptane flame due to the presence of CO_2, although it still is quite small for $\chi_{st} = 1$ s^{-1}. Because of the marginal contribution of absorption for the hydrogen flame, the net radiative loss predicted by the gray model (plotted as circles in Fig. 7) is comparable to that

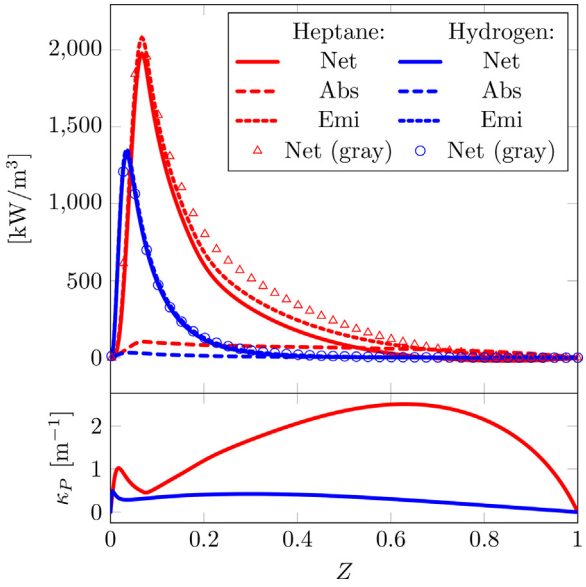

Fig. 7. Net radiative losses for the heptane and hydrogen flames ($\chi_{st} \approx 1.0$ s^{-1}).

of the non-gray model; the same is not observed for the heptane flame. The good agreement between gray and non-gray solutions for the hydrogen flame has been observed throughout the S-curve, with exception of a small region near the lower extinction limit. This indicates that the requirement for spectral modeling may be less stringent for hydrogen flames compared to hydrocarbon ones, and a gray medium approach (or even the OTA) may suffice in some cases. Similar findings have been reported in the literature, see, e.g., Refs. [4,29].

Note also that, differently from the heptane flame, the Planck-mean absorption coefficient of the hydrogen flame, also plotted in Fig. 7, varies little with the mixture fraction. This likely occurs due to the lack of CO_2 in the flame, which is a strongly absorbing species that appears both in the lean and rich regions of the heptane flame, as shown by the two peaks in the κ_P plot for that flame. The relatively flat distribution of the Planck-mean absorption coefficient with respect to Z for the hydrogen flame further suggests that simpler spectral radiation models may be adequate for H_2 combustion.

5. Discussions

When employing classical RTE solution methods (e.g., discrete ordinates method and spherical harmonics), or when using the one-dimensional non-local model introduced in this paper, the operations related to the solution of Eq. (2) for the radiative intensity have by far the largest share of the cost associated to the determination of the radiation field. In contrast, the calculation of the radiative properties of the medium has a negligible cost, since it usually involve the computation of simple functions or interpolations of data from look-up tables. Therefore, the number of times that the RTE needs to be solved is, to a good approximation, directly related to the overall cost of the radiation solver; i.e., the gray medium approach, that requires that the RTE be solved a single time along each optical path at any given call to the radiation solver, requires one fourth of the cost of the non-gray, four-gray gas WSGG model employed in the present study (or one fifth if the transparent windows are to be considered, as it would be necessary to compute radiative heat fluxes in enclosures formed by differently-heated walls, for example). This imposes a significant constraint on the choice of a non-gray radiation model, since more sophisticated models as a rule entail even more consecutive solutions of the RTE—in the limit of the most accurate spectral treatment available, the LBL integration method requires hundreds of thousands to millions of RTE solutions for each optical path.

The issue of computational cost is the main reason why the gray medium assumption (or the OTA, which foregoes the solution of the RTE completely) is common in coupled combustion calculations. These simplified radiation models are sufficient for optically thin flame conditions, as it was verified in Sections 4.1 and 4.2 for the atmospheric heptane flame near the upper extinction limit burning at standard-air or reduced oxygen concentrations, and in Section 4.3 for the hydrogen flame throughout most of its S-curve. This is further illustrated in Fig. 8(a) and (b), where the error of the gray, non-local model solution (relative to the non-gray one) in the prediction of the maximum temperature is plotted as a function of the stoichiometric scalar dissipation rate across the upper branch of the S-curve for all cases considered in Section 4. For the aforementioned conditions, $T_{\max}$ computed assuming a gray medium is within 5% of the result obtained by the non-gray approach. The accuracy of the OTA is similar to that of the gray solution for these optically thin flame scenarios, as noted previously.

It should be noted, however, that the gray solution is generally not capable of accurately approximating the radiation field even in the optically thin region. This is evidenced by Fig. 8(c) and (d), which depict the error of that solution for the domain-integrated net radiative loss $Q_{net} = -2\pi \int_0^R S_r r dr$. With exception of the hydrogen flame, whose error in the prediction of Q_{net} is approximately 3% near the upper extinction limit, the domain-integrated radiative loss is overestimated by at least 20% for all other flames. This is consistent with what is widely reported in the literature regarding the accuracy of the gray assumption for modeling gaseous media [6]. Nevertheless, the large error of the gray solution in the prediction of the radiation field is not translated into comparable errors in the prediction of scalars such as the temperature near the upper extinction limit because radiation itself is not important in that region of the S-curve, cf. the radiant fraction plots reported in Fig. 8(e) and (f).

As χ_{st} decreases and the flame nears its lower extinction point, the importance of radiation increases significantly, with the radiant fraction surpassing 0.7 for the high-pressure and hydrogen flames. The optical thickness also increases, driven mainly by the broadening of the flame. Therefore, the gray solution leads to significant errors in the calculation of $T_{\max}$, as much as 30% close to the lower extinction limit. For the reasons discussed in Section 4.3, the accuracy of the gray model for the hydrogen flame tends to be better than that for the heptane flame at comparable conditions.

Note, however, that Fig. 8 only compares regions of the S-curve where both gray and non-gray models produce a solution, and thus it does not capture the effect that the choice of spectral treatment has on the extinction point. This is particularly important for flames under reduced oxygen concentrations, where the use of a gray model predicts that extinction occurs at a significantly larger stoichiometric scalar dissipation rate (cf. Fig. 5). In the most critical scenario, for the heptane flame burning at 11.0% oxygen concentration, extinction occurs at $\chi_{st} = 0.022$ s^{-1} for the gray solution (and 0.021 s^{-1} for the OTA), whereas for the non-gray solution the flame persists all the way to $\chi_{st} = 0.007$ s^{-1}.

Using the non-local model, recommendations on spectral model selection may be drawn from simple simulations such as the ones carried out in Section 4, as long as one provides a description of the combustion conditions of interest—e.g., fuel and oxidizer compositions, pressure, and size of the burner. In addition, for non-radiation experts, the model may simplify the selection of an adequate treatment for radiation. In Section 4, it was shown that findings regarding the radiation characteristics of different flames made on the basis of the non-local model agree with previous works in the literature. However, whereas those traditional inves-

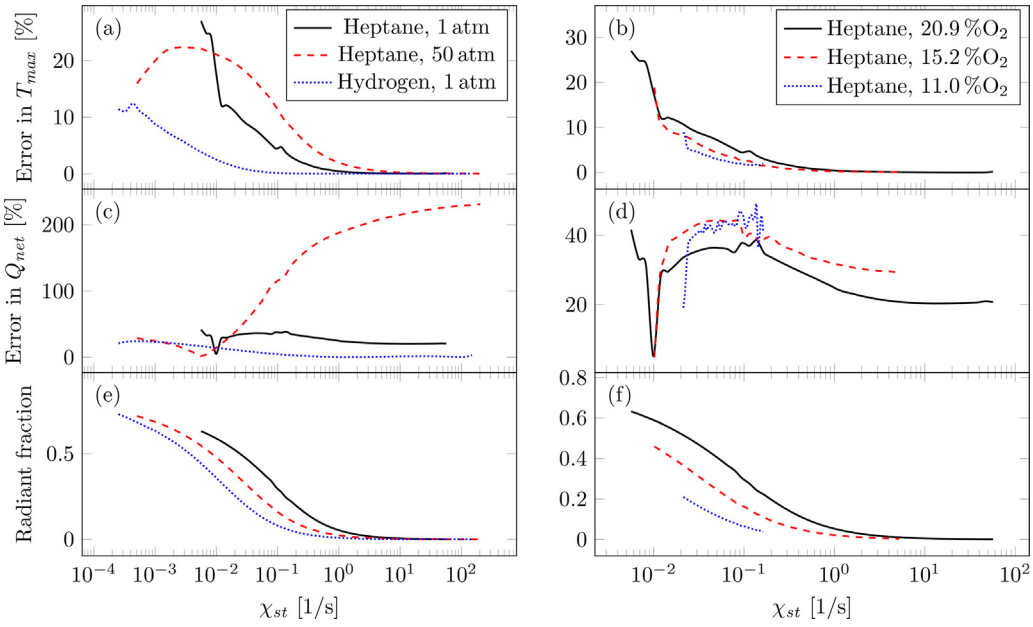

Fig. 8. Errors of the gray solution, relative to the non-gray one, in the predictions of maximum temperature (a,b) and domain-integrated radiative loss (c,d), and radiant fraction of the flame (e,f), across the upper branch of the S-curve for the cases considered in Section 4.

tigations of radiation modeling in combustion systems required expensive multidimensional calculations, the non-local model is a straightforward and computationally efficient approach to reach similar conclusions.

Finally, it should be noted that the non-local model has only been employed for conical-shaped diffusion flames so far. For flames that significantly deviate from a cylindrical or conical topology, the model might require further development, although local perturbations from these shapes are already permissible to some degree. Moreover, testing with the model has been limited to small-scale flames, and extension to large-scale flames requires further study. Lastly, the non-local model has been prescribed with scalar profiles from either laminar or highly-resolved turbulent simulations. Accuracy of the model in situations where only low-resolution data are available still requires further studies.

6. Conclusions

A one-dimensional non-local model for computing radiative self-absorption in flames was derived in this study and used to provide radiation modeling recommendations for combustion applications. The model approximates the flame structure as an infinitely long cylinder where properties only vary along the radial direction. Flamelet solutions in the composition space are then mapped into the physical space, from which the radiative absorption and the net radiative loss may be determined analytically. By selecting appropriate flamelets, the non-local model can be used to represent non-premixed and premixed flames under various working conditions.

The model was first validated for a laminar methane/air jet flame and a turbulent heptane pool fire. Radial profiles of temperature and species concentrations at different heights were extracted from fully-coupled, multidimensional simulations of these flames and used as input to the non-local model. Good agreement in the predicted net radiative heat loss and the self-absorption was observed between the non-local model and the reference multidimensional simulation.

Next, the non-local model was applied in three different cases to illustrate how it can be employed to provide radiation modeling recommendations for combustion simulations. First, atmospheric and pressurized heptane/air flames were compared, and the results of the model demonstrated the increased significance of radiation self-absorption at the higher pressure due to the increase in optical thickness. In addition, accounting for non-gray effects was shown to be critical particularly at high pressures. Second, a fire suppression scenario with reduced oxygen content was considered. Comparisons of the S-curve showed that the choice of the radiation model modifies the lower extinction limit, and the need for an accurate spectral radiation treatment becomes more significant as the oxygen concentration decreases. Finally, a hydrogen/air flame was studied. The absence of carbon dioxide was found to reduce the net radiative loss and the flame self-absorption, and to reduce the variations of the Planck-mean absorption coefficient with respect to the mixture fraction. Compared to heptane flames at similar conditions, the optical thickness of hydrogen flames was smaller and the importance of non-gray radiation was also reduced, indicating that the radiation modeling requirements are potentially less stringent for these flames.

The findings reported in the present paper are consistent with observations in the literature from multidimensional radiation-combustion simulations in more realistic geometries. This shows the potential of the one-dimensional non-local model as an effective and computationally inexpensive tool for selecting radiation modeling approaches for combustion applications. Notice also that, because the non-local model is capable of accurately approximating the radiative absorption in realistic flames based solely on flamelet data, it is an attractive option for including self-absorption effects in flamelet-generated manifold models. This point will be explored in a future study.

Declaration of Competing Interest

The authors declare that they have no known competing financial interests or personal relationships that could have appeared to influence the work reported in this paper.

Acknowledgments

The authors acknowledge funding support by FM Global within the framework of the FM Global Strategic Research Program on Fire Modeling.

Supplementary material

Supplementary material associated with this article can be found, in the online version, at doi:10.1016/j.combustflame.2023.112907.

References

[1] R. Viskanta, Radiative Transfer in Combustion Systems: Fundamentals and Applications, Begell House, New York, USA; Wallingford, UK, 2005.

[2] Y. Ju, G. Masuya, P.D. Ronney, Effects of radiative emission and absorption on the propagation and extinction of premixed gas flames, Symp. (Int.) Combust. 27 (2) (1998) 2619–2626, doi:10.1016/s0082-0784(98)80116-1.

[3] S. Mazumder, M.F. Modest, A probability density function approach to modeling turbulence–radiation interactions in nonluminous flames, Int. J. Heat Mass Transf. 42 (6) (1999) 971–991, doi:10.1016/s0017-9310(98)00225-7.

[4] J. Frank, R. Barlow, C. Lundquist, Radiation and nitric oxide formation in turbulent non-premixed jet flames, Proc. Combust. Inst. 28 (1) (2000) 447–454, doi:10.1016/s0082-0784(00)80242-8.

[5] G. Li, M.F. Modest, Importance of turbulence-radiation interactions in turbulent diffusion jet flames, J. Heat Transf. 125 (5) (2003) 831–838, doi:10.1115/1.1597621.

[6] M.F. Modest, D.C. Haworth, Radiative Heat Transfer in Turbulent Combustion Systems: Theory and Applications, Springer, 2016.

[7] M.F. Modest, Radiative Heat Transfer, third ed., Academic Press, 2013.

[8] V.P. Solovjov, B.W. Webb, F. Andre, Radiative properties of gases, Handbook of Thermal Science and Engineering, Springer (2018), pp. 1069–1141, doi:10.1007/978-3-319-26695-4_59.

[9] J.R. Howell, M.P. Mengüç, K. Daun, R. Siegel, Thermal Radiation Heat Transfer, seventh ed., CRC Press, 2021.

[10] B. Wu, M. Ihme, X. Zhao, Limitations of flamelet formulation for modeling turbulent pool fires, Combust. Flame 227 (2021) 346–358.

[11] F.H. Azad, M.F. Modest, Evaluation of the radiative heat flux in absorbing, emitting and linear-anisotropically scattering cylindrical media, J. Heat Transf. 103 (2) (1981) 350–356.

[12] N.W. Bressloff, J.B. Moss, P.A. Rubini, Assessment of a differential total absorptivity solution to the radiative transfer equation as applied in the discrete transfer radiation model, Numer. Heat Transf., Part B 29 (3) (1996) 381–397.

[13] F. Liu, H.A. Becker, Y. Bindar, A comparative study of radiative heat transfer modelling in gas-fired furnaces using the simple grey gas and the weighted–sum-of-grey-gases models, Int. J. Heat Mass Transf. 41 (22) (1998) 3357–3371.

[14] P.J. Coelho, Numerical simulation of radiative heat transfer from non-gray gases in three-dimensional enclosures, J. Quant. Spectrosc. Radiat. Transf. 74 (3) (2002) 307–328.

[15] G.C. Fraga, L. Zannoni, F.R. Centeno, F.H.R. França, Evaluation of different gray gas formulations against line-by-line calculations in two- and three-dimensional configurations for participating media composed by CO_2, H_2O and soot, Fire Saf. J. 108 (2019) 102843.

[16] M.F. Modest, The weighted-sum-of-gray-gases model for arbitrary solution methods in radiative transfer, J. Heat Transf. 113 (3) (1991) 650–656, doi:10.1115/1.2910614.

[17] M.H. Bordbar, G. Wecel, T. Hyppänen, A line by line based weighted sum of gray gases model for inhomogeneous CO_2-H_2O mixture in oxy-fired combustion, Combust. Flame 161 (9) (2014) 2435–2445.

[18] H. Bordbar, F.R. Coelho, G.C. Fraga, F.H.R. França, S. Hostikka, Pressure-dependent weighted-sum-of-gray-gases models for heterogeneous CO_2-H_2O mixtures at sub- and super-atmospheric pressure, Int. J. Heat Mass Transf. 173 (2021) 121207.

[19] F.R. Coelho, F.H.R. França, WSGG correlations for H_2O and CO_2 in high pressure conditions, Procceedings of the 24th ABCM International Congress of Mechanicl Engineering, ABCM, 2017.

[20] R.B. Miguel, I.M. Machado, F.M. Pereira, P.R. Pagot, F.H.R. França, Application of inverse analysis to correlate the parameters of the weighted-multi-point-source model to compute radiation from flames, Int. J. Heat Mass Transf. 102 (2016) 816–825, doi:10.1016/j.ijheatmasstransfer.2016.06.051.

[21] B. Wu, X. Zhao, Effects of radiation models on steady and flickering laminar non-premixed flames, J. Quant. Spectrosc. Radiat. Transf. 253 (2020) 107103, doi:10.1016/j.jqsrt.2020.107103.

[22] S. James, M.S. Anand, M.K. Razdan, S.B. Pope, In situ detailed chemistry calculations in combustor flow analyses, J. Eng. Gas Turbines Power 123 (4) (1999) 747–756, doi:10.1115/1.1384878.

[23] L.S. Rothman, I.E. Gordon, R.J. Barber, H. Dothe, R.R. Gamache, A. Goldman, V.I. Perevalov, S.A. Tashkun, J. Tennyson, HITEMP, the high-temperature molecular spectroscopic database, J. Quant. Spectrosc. Radiat. Transf. 111 (15) (2010) 2139–2150, doi:10.1016/j.jqsrt.2010.05.001.

[24] A. Wang, M.F. Modest, Spectral Monte Carlo models for nongray radiation analyses in inhomogeneous participating media, Int. J. Heat Mass Transf. 50 (19–20) (2007) 3877–3889, doi:10.1016/j.ijheatmasstransfer.2007.02.018.

[25] W.L. Chan, H. Kolla, J.H. Chen, M. Ihme, Assessment of model assumptions and budget terms of the unsteady flamelet equations for a turbulent reacting jet-in-cross-flow, Combust. Flame 161 (10) (2014) 2601–2613, doi:10.1016/j.combustflame.2014.04.007.

[26] H. Pitsch, A C++ computer program for 0D combustion and 1D laminar flame calculations, 1990.

[27] T. Lu, A reduced/skeletal n-heptane model for high temperature condition (JetSurF 1.0-1), Pers. Commun.2019.

[28] M.Ó. Conaire, H.J. Curran, J.M. Simmie, W.J. Pitz, C.K. Westbrook, A comprehensive modeling study of hydrogen oxidation, Int. J. Chem. Kinet. 36 (11) (2004) 603–622, doi:10.1002/kin.20036.

[29] J. Cai, S. Lei, A. Dasgupta, M.F. Modest, D.C. Haworth, High fidelity radiative heat transfer models for high-pressure laminar hydrogen-air diffusion flames, Combust. Theor. Model. 18 (6) (2014) 607–626, doi:10.1080/13647830.2014.959060.

[30] F. Nmira, J.-L. Consalvi, F. André, Pressure effects on radiative heat transfer in hydrogen/air turbulent diffusion flames, J. Quant. Spectrosc. Radiat. Transf. 220 (2018) 172–179, doi:10.1016/j.jqsrt.2018.09.013.

[31] C. Paul, S.F. Fernandez, D.C. Haworth, S. Roy, M.F. Modest, A detailed modeling study of radiative heat transfer in a heavy-duty diesel engine, Combust. Flame 200 (2019) 325–341, doi:10.1016/j.combustflame.2018.11.032.

[32] A.L. Johnson, X. Zhao, Analysis of the heat transfer within combustor liners using a combined Monte Carlo and two-flux method, J. Turbomach. 143 (3) (2021), doi:10.1115/1.4049913.

[33] N. Ren, D. Zeng, K.V. Meredith, Y. Wang, S.B. Dorofeev, Modeling of flame extinction/re-ignition in oxygen-reduced environments, Proc. Combust. Inst. 37 (3) (2019) 3951–3958, doi:10.1016/j.proci.2018.06.076.